ARTICLE

Multi-Physics Modeling of Solid Oxide Fuel Cell Fueled by Methane and Analysis of Carbon Deposition

Bao-xuan Wang[a], Jiang Zhu[a], Zi-jing Lin[a,b*]

a. Hefei National Laboratory for Physical Sciences at the Microscale & Collaborative Innovation Center of Suzhou Nano Science and Technology, University of Science and Technology of China, Hefei 230026, China

b. Key Laboratory of Strongly-Coupled Quantum Matter Physics, Chinese Academy of Sciences, and Department of Physics, University of Science and Technology of China, Hefei 230026, China

(Dated: Received on March 9, 2015; Accepted on April 14, 2015)

Internal reformation of low steam methane fuel is important for the high efficiency and low cost operation of solid oxide fuel cell. Understanding and overcoming carbon deposition is crucial for the technology development. Here a multi-physics model is established for the relevant experimental cells. Balance of electrochemical potentials for the electrochemical reactions, generic rate expression for the methane steam reforming, dusty gas model in a form of Fick's model for anode gas transport are used in the model. Excellent agreement between the theoretical and experimental current-voltage relations is obtained, demonstrating the validity of the proposed theoretical model. The steam reaction order in low steam methane reforming reaction is found to be 1. Detailed information about the distributions of physical quantities is obtained by the numerical simulation. Carbon deposition is analyzed in detail and the mechanism for the coking inhibition by operating current is illustrated clearly. Two expressions of carbon activity are analyzed and found to be correct qualitatively, but not quantitatively. The role of anode diffusion layer on reducing the current threshold for carbon removal is also explained. It is noted that the current threshold reduction may be explained quantitatively with the carbon activity models that are only qualitatively correct.

Key words: Numerical model, Methane reforming kinetics, Current-voltage relation, Carbon activity, Diffusion barrier layer

I. INTRODUCTION

Solid oxide fuel cell (SOFC) has gained significant attention in recent decades due to its high energy efficient and fuel flexibility. Because of its high operating temperature (600−800 °C), SOFC can operate directly with carbon-based fuels [1], such as methane that is low-cost and convenient for storage. As only hydrogen and carbon monoxide may be active in the electrochemical oxidation reactions, methane needs to be reformed [2]. The reforming reactions may be carried out inside the cell, and this internal reforming (IR) is attractive due to the benefits: external reforming components are eliminated with the reduced system complexity and cost, products and heat released by the electrochemical reactions may be used for the reforming reactions with the improved system efficiency and performance [2, 3]. However, IR brings extra complexities: carbon deposition may occur in the anode and destroy the cell quickly; the cooling effect of the endothermic reforming reactions may lead to large temperature gradients, causing the cell to crack or delaminate [4, 5]. Avoiding carbon deposition and high temperature gradient is important for the success of SOFC fueled with methane.

An anode-support planar SOFC has a relatively thick porous anode, usually composed of nickel and yttria-stabilized zirconia (YSZ) [6]. Besides good electrochemical performance, nickel has high catalytic activities in methane reforming reactions and water-gas shift reactions [7−9]. However, nickel also has a high catalytic activity in methane cracking reaction and Boudard reaction, which are the major pathways for carbon deposition [10]. Many efforts have been made to avoid the coke formation. Adding steam or carbon dioxide to methane is helpful for reducing the thermodynamic tendency of the coke formation [3, 11], but has the drawback of the reduced Nernst potential and system performance. It is reported that changing the anode catalyst such as complete or partial replacement of Ni by Cu or Co or impregnation of doped ceria can reduce the risk of coke formation [12, 13]. Another way to suppress the coke formation is to operate the SOFC with an adequately high current [6]. The current threshold may be lowered

*Author to whom correspondence should be addressed. E-mail: zjlin@ustc.edu.cn, Tel.: +86-551-63600345, FAX: +86-551-63606348

by introducing a diffusion layer between the fuel flow and Ni-YSZ anode [14]. However, the mechanism for the suppression of coke formation by the current and the diffusion layer is not well understood. Research effort is required for understanding the mechanism that is important for advancing the methane fueled SOFC technology.

Mathematical modeling is playing an increasingly important role in the investigations of SOFCs due to its cost effectiveness and clear illustrations of the physical processes and mechanisms. Indeed, there have been a number of modeling studies on methane fueled SOFCs [3, 15, 16]. Unfortunately, none of these simulations has considered the effect of methane reforming on the Nernst potential. Consequently, the governing equations are only applicable to methane with high steam content at the best. Moreover, the existing modeling results show that the distributions of gas components affect significantly the performance of SOFCs [17, 18]. An accurate description of methane transport in the porous anode is important for the reliability of modeling result. Replacing the commonly used Fick's law for the mass transport in the anode with a tested accurate model such as the dusty gas model (DGM) [19, 20] or its equivalent [21] is highly desirable.

Here, we report the results of a multi-physics modeling of a methane fueled button SOFC. The effect of IR on the electrochemistry is properly taken into account by employing the equations based on the balance of electrochemical potentials that are fuel composition dependent. The mass transport of methane fuel is described by the so-called DGMFM model that is shown to be equally accurate as the DGM model [21]. Detailed analysis of the distributions of physical quantities such as temperature and gas composition in the anode is carried out. The thermodynamic possibility of carbon deposition in connection with the operating current density is discussed. Impacts of inlet fuel composition on the cell performance are also examined. Finally, the effect of diffusion layer on the carbon deposition activity is analyzed.

II. THEORETICAL METHOD

A new multi-physics mathematical model of methane fueled SOFC is developed that consists of the following main components: (i) Kinetic rate equation for methane steam reforming reaction (STR) in the anode to be described below. (ii) Water-gas shift (WGS) reaction, $CO+H_2O=H_2+CO_2$, assumed to be in quasi-equilibrium, (iii) Mass, momentum and energy transport in the gas chamber determined by the conventional computational fluid dynamics (CFD), as described before [22]. (iv) Mass, momentum and energy transport in the porous electrode. The governing equations for the momentum and energy transports are the same as that described in Ref.[22], but the DGMFM model [21] is used for the fuel mass transport in the anode. (v) Governing equations for the electrochemical potential balance, as described in Ref.[23]. (vi) Ohm's law for the transport of electronic and ionic current inside the cell [23]. (vii) Butler-Volmer equation for the electrochemical reaction at the triple-phase boundary (TPB) region, as described in detail before [22, 23]. (viii) Energy sources due to the STR and WGS reactions, electrochemical activation reaction, electronic and ionic current conduction as described in Refs.[22−24].

In short, the newly developed mathematical model combines the theoretical models of Refs.[21−24] with the following STR rate equation:

$$r_{\rm STR} = k_{\rm STR} p_{\rm CH_4}^m p_{\rm H_2O}^n \exp\left(-\frac{E_{\rm a}}{RT}\right) \cdot \left(1 - \frac{p_{\rm H_2}^3 p_{\rm CO}}{p_{\rm CH_4} p_{\rm H_2O} K_{\rm eq,STR}}\right) \quad (1)$$

According to the experimental measurement of Ref.[25], m=1, $k_{\rm STR}$=9.46×10^7 mol/(m^3·s·bar), $E_{\rm a}$= 96.1 kJ/mol. The steam reaction order, n, for the STR reaction is not preset and may vary between 0 and 1. However, n is verified to be 1 by comparison with the experiment using low stream content methane fuel. Moreover, a multiplier constant, $\overline{k}_{\rm STR}$, is introduced for the prefactor to reflect the influence of the catalyst used. That is, the STR rate equation for low steam methane fuel is expressed as,

$$r_{\rm STR} = 9.46\times10^7 \overline{k}_{\rm STR} p_{\rm CH_4} p_{\rm H_2O} \exp\left(-\frac{96.1}{RT}\right) \cdot \left(1 - \frac{p_{\rm H_2}^3 p_{\rm CO}}{p_{\rm CH_4} p_{\rm H_2O} K_{\rm eq,STR}}\right) \quad (2)$$

where $\overline{k}_{\rm STR}$ is to be determined by fitting to the experimental result. The equilibrium constant for the STR reaction is known [26, 27] to be $K_{\rm eq,STR}$= $1.198\times10^{17}\exp(-26830K/T)$ (kPa)^2.

The above described mathematical model is applied to the button cell experiments reported in Refs.[6, 28, 29], together with the macro and micro structural and property parameters indicated in the corresponding experiments. The basic structural and operating parameters for the numerical modeling are listed in Table I. Due to the symmetry of the button cells, a button cell with a gas chamber at the anode side is structured in a two-dimensional (2D) axisymmetric computational domain, as illustrated in Fig.1. In Fig.1 two positions are marked out specifically for the convenience of analysis. The two representative positions are the center of the interface between the electrolyte and anode (position O_A), and the center of the surface of anode (position O_B).

The boundary conditions for solving the above described coupled partial differential equations (PDEs) are set in accordance with the experimental operation. For the anode side, a molar flux boundary coupled with

DOI:10.1063/1674-0068/28/cjcp1503033

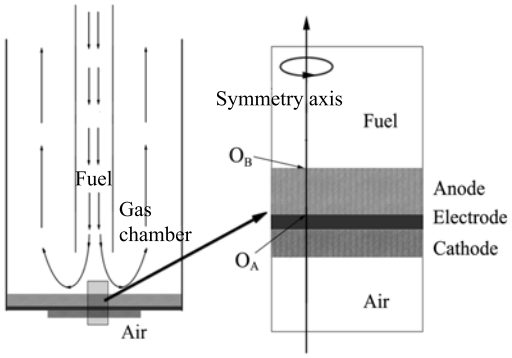

FIG. 1 Geometric schematic for the 2D axisymmetric computational domain of experimental button cells.

TABLE I Basic structural and material parameters and operating conditions used in the numerical modeling [6, 15, 28].

Anode thickness	0.5 mm
Anode diameter	20 mm
YSZ volume fraction in anode	0.65
Electrolyte thickness	25 μm
Cathode thickness	30 μm
Cathode area	0.5 cm^2
YSZ volume fraction in cathode	0.52
Porosity ϕ	0.35
Tortuosity τ	3.8
Average pore radius r_g	0.5 μm
Average particle diameter d_p	1 μm
Thickness of diffusion barrier layer	500 μm
Fuel flow rate (humidified CH_4)	50 sccm
Fuel flow rate (humidified H_2)	100 sccm
Molar fraction of H_2O in fuel	0.03
External temperature T_0	600, 650, 700, 750, 800 °C
External pressure P_0	1 atm

laminar inflow is used at the fuel inlet, where the temperature is set as T_0; an outflow boundary with pressure of P_0 is used at the fuel outlet; and other boundaries are set as no slip wall. The cathode is exposed to ambient air, a concentration boundary is set for mass transport, and a convective cooling boundary is for heat transport, with an external temperature T_0 and a heat transfer coefficient h=100 W/(m^2·K) [30]. At the interfaces between the electrolyte and electrodes, the boundary conditions of no slip wall and molar sources are set for the gas transport, continuous temperature is set for heat transport, and continuous voltage is set for the charge transport. The alumina tubes which support the cell are assumed to be insulating.

The model is performed in the finite element commercial software COMSOL MULTIPHYSICS® Version 3.5 [31]. The computational domain is meshed by mapped grids, where 50000 degrees of freedom are included, and a stationary direct nonlinear solver UMFPACK is used to solve the discretized PDEs.

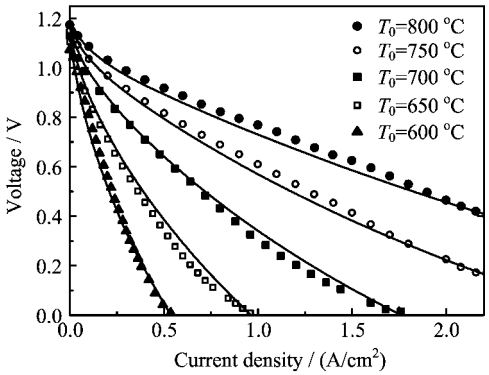

FIG. 2 Comparison between theoretical (solid lines) and experimental (scatters) I-V relations of a button cell fueled by humidified CH_4 [6].

III. RESULTS AND DISCUSSION

A. Model validation and reaction kinetics for low steam methane reforming

The theoretical method described above has been used to calculate the temperature dependent current-voltage (I-V) relations that have been measured experimentally. With the operating parameters specified in the experiments [6, 14, 28], good agreements between the experimental and theoretical I-V relations may be obtained with $\overline{k}_{STR}$=8, as shown in Fig.2. The agreements between the theoretical and experimental I-V relations are highly satisfactory, confirming the validity of the used multi-physics electrochemistry model.

It is interesting to note that the I-V relation is not very sensitive to the value of $\overline{k}_{STR}$. Changing $\overline{k}_{STR}$ by a factor of two, *i.e.*, from 8 to 4 or 16, only moderately affects the quality of theoretical and experimental agreement. On the other hand, the I-V relation is substantially affected by the steam reaction order (n) for the methane steam reforming. No reasonable theoretical and experimental agreement may be obtained if n is changed from 1 to 0 (as often observed for high steam methane fuel). In fact, the agreement for n=0.8 or 1.2 is notably poorer than that for n=1. In other words, it is fairly accurate to conclude that the steam reaction order of the methane steam reforming is 1 when the steam content is low.

The sensitivity (insensitivity) of the I-V relation to n ($\overline{k}_{STR}$) for low steam methane fuel is understandable. Due to the consumption of H_2O in the reforming reaction, P_{H_2O} is in the order of 10^{-3} bar inside the anode. Changing n by 0.2 or more is equivalent to changing the reaction rate (Eq.(1)) by a factor of 4 or more, while changing $\overline{k}_{STR}$ by a factor of 2 only affects the reaction

DOI:10.1063/1674-0068/28/cjcp1503033

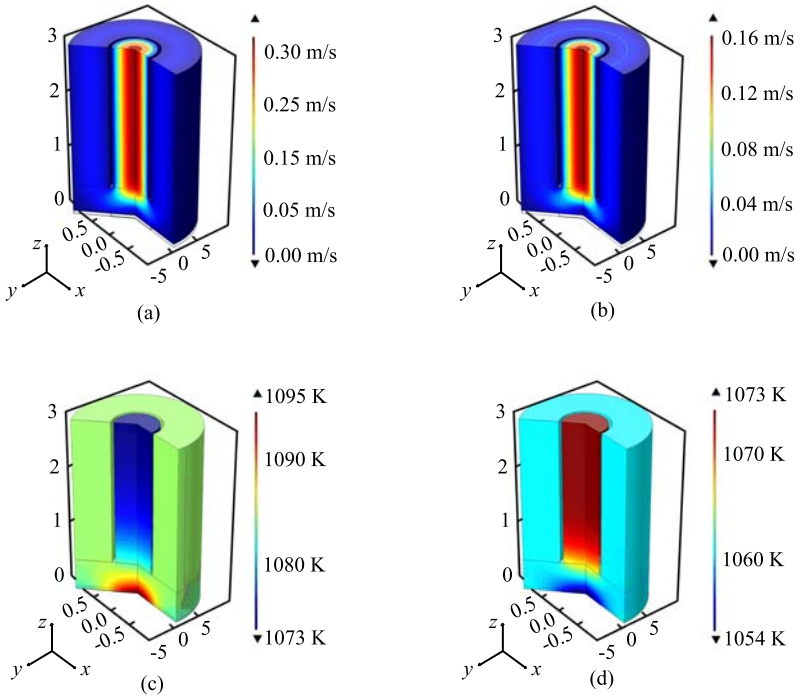

FIG. 3 Distributions of flow and temperature. (a) Flow velocity distribution of H_2 fueled cell, (b) flow velocity distribution of CH_4 fueled cell, (c) temperature of H_2 fueled cell, and (d) temperature of CH_4 fueled cell.

rate by a factor of 2.

In short, from the comparison of the theoretical and experimental *I-V* relations it not only validates the adopted theoretical model, but also concludes that Eq.(2) is the only reasonable kinetic rate expression for low steam methane reforming reaction.

B. Distributions of fuel flow, temperature, and chemical reaction rate

Figure 3 shows the flow field in the gas chamber and temperature distribution of the whole cell with both humidified CH_4 and H_2 fuels at T_0=800 °C and the output current density, $i_{\rm out}$, of 1.5 A/cm^2. Similar flow patterns are found for the CH_4 and H_2 fuels, but subtle difference exists. In the methane fueled cell, some extra flow due to the reforming reaction is generated from the anode.

On the other hand, characteristically different temperature distributions are observed for the CH_4 and H_2 fuels due to the balance of the exothermic electrochemical reaction and the endothermic reforming reaction. The temperature of the hydrogen fueled cell is higher than T_0 as only the exothermic electrochemical reaction is involved. The temperature for the methane fueled button cell is lower than T_0 as heat generated by the electrochemical reaction is less than that consumed by the reforming reaction at the discussed operating condition.

Due to the low ionic conductivity of electrodes, only a narrow region of the anode neighboring the electrolyte is electrochemical activated. This is the case for both hydrogen and methane fuels, as may be easily seen in Fig.4(a). However, the temperature profiles for H_2 and CH_4 fuels are characteristically different. The temperatures at O_A for different fuels and operating conditions are presented in Fig.4(b). Clearly, the temperature at O_A rises with the current density for the hydrogen fueled cell. For the methane fueled cell, the temperature drops with the increasing current density at first due to the overwhelming endothermic reforming reaction, then rises with the increased current due to the increased heat generation by the electrochemical and ohmic processes. As seen in Fig.4(b), the electrochemical heat generation may be used effectively by the methane reforming reaction. This feature is very helpful for improving the energy efficiency of methane fueled SOFCs.

Figure 5 shows the heat fluxes by thermal conduction and gas convection at the symmetry axis for $i_{\rm out}$=1.5 A/cm^2, T_0=800 °C and methane fuel. Note that, though the solid conduction plays a major role in the heat transfer, the convective heat transfer is also important. An accurate description of gas flow in the porous electrode is of importance as the total heat flux is the balance of the conductive and convective heat flues and is sensitive to the error in evaluating the convective heat flux. Therefore, the use of DGM or DGMFM for the gas transport is recommendable, but the use of Fick's law is discouraging.

DOI:10.1063/1674-0068/28/cjcp1503033

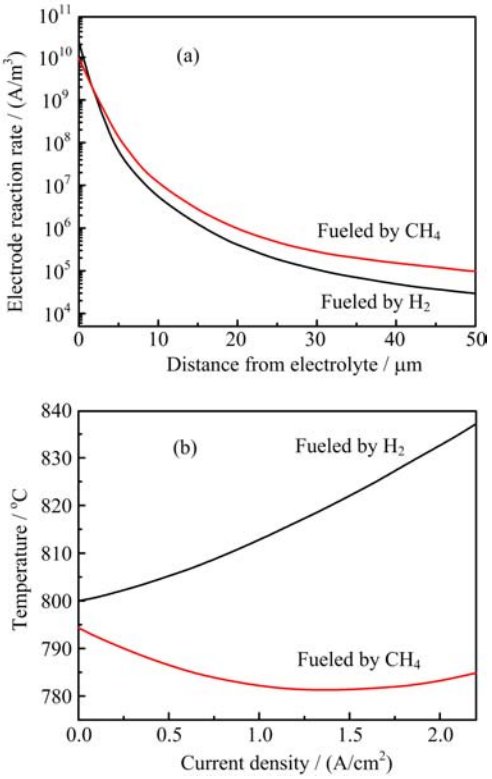

FIG. 4 Effect of fuel on the electrochemical reaction and cell temperature. (a) Electrochemical reaction rate at the anode symmetry axis for i_{out}=1.5 A/cm^2 and T_0=800 °C. (b) Dependence of temperature at O_A on current density, T_0=800 °C.

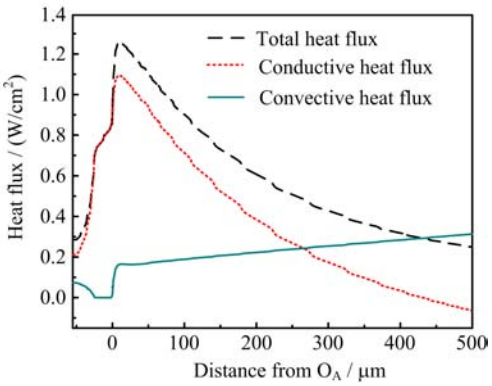

FIG. 5 Heat fluxes of thermal conduction and gas convection at the symmetry axis for i_{out}=1.5 A/cm^2, T_0=800 °C and methane fuel.

C. Fuel compositions and carbon deposition

Figure 6 illustrates the distributions of fuel compositions on the anode symmetry axis. As shown in Fig.6, the methane concentration is the highest on the anode surface, where the steam content is the lowest. Clearly, the anode surface is the most likely place for carbon deposition and O_B (the center of the anode surface, see

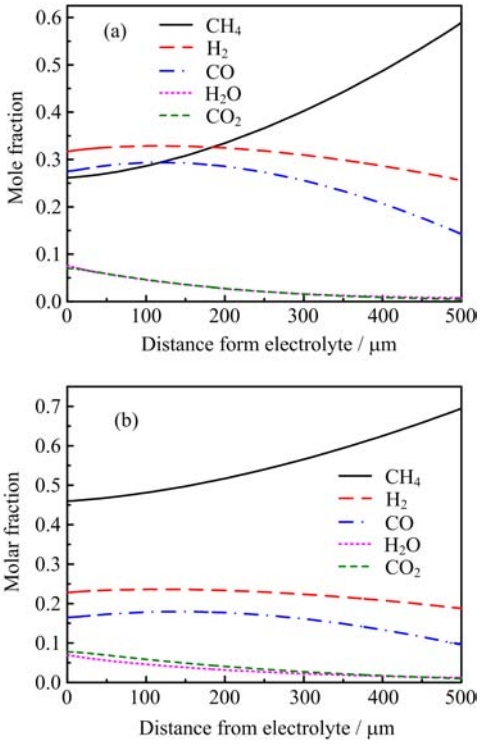

FIG. 6 Fuel compositions on the anode symmetry axis. (a) i_{out}=1.5 A/cm^2, T_0=800 °C, (b) i_{out}=1.0 A/cm^2, T_0=700 °C.

Fig.1) is used as the representative location in the following discussion of carbon deposition.

Fuel compositions at O_B are shown in Fig.7. The methane content decreases while other fuel compositions increase with the increased output current, the tendency of carbon deposition through the Boudard reaction, CH_4=C+2H_2, therefore decreases, in good accordance with the experimental observation of carbon inhibition by operating current [4, 6, 11, 29].

The thermodynamic tendency of carbon deposition may be expressed as the carbon activity [4, 11, 32−34]. There are two reaction routes related to the carbon formation: (i) CH_4=C+2H_2 and (ii) 2CO=C+CO_2. The corresponding carbon activities may be expressed as,

$$a_{C,CH_4} = k_{eq,1}\frac{p_{CH_4}}{p_{H_2}^2} \quad (3)$$

$$a_{C,CO} = k_{eq,2}\frac{p_{CO}^2}{p_{CO_2}} \quad (4)$$

where a_{c,CH_4} and $a_{c,CO}$ are the carbon activity via the reaction (i) and (ii), respectively. The chemical equilibrium constants may be evaluated as [26, 27],

$$k_{eq,i} = 4.161\times10^7 \exp\left(\frac{-10614K}{T}\right) \quad (5)$$

$$k_{eq,ii} = 5.744\times10^{-12} \exp\left(\frac{20634K}{T}\right) \quad (6)$$

DOI:10.1063/1674-0068/28/cjcp1503033

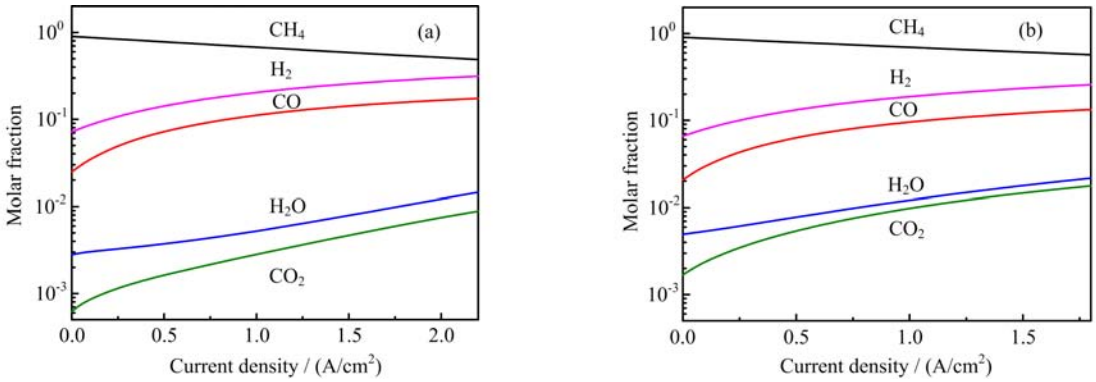

FIG. 7 Variations of fuel compositions at O_B with the cell output current density. (a) T_0=800 °C, (b) T_0=700 °C.

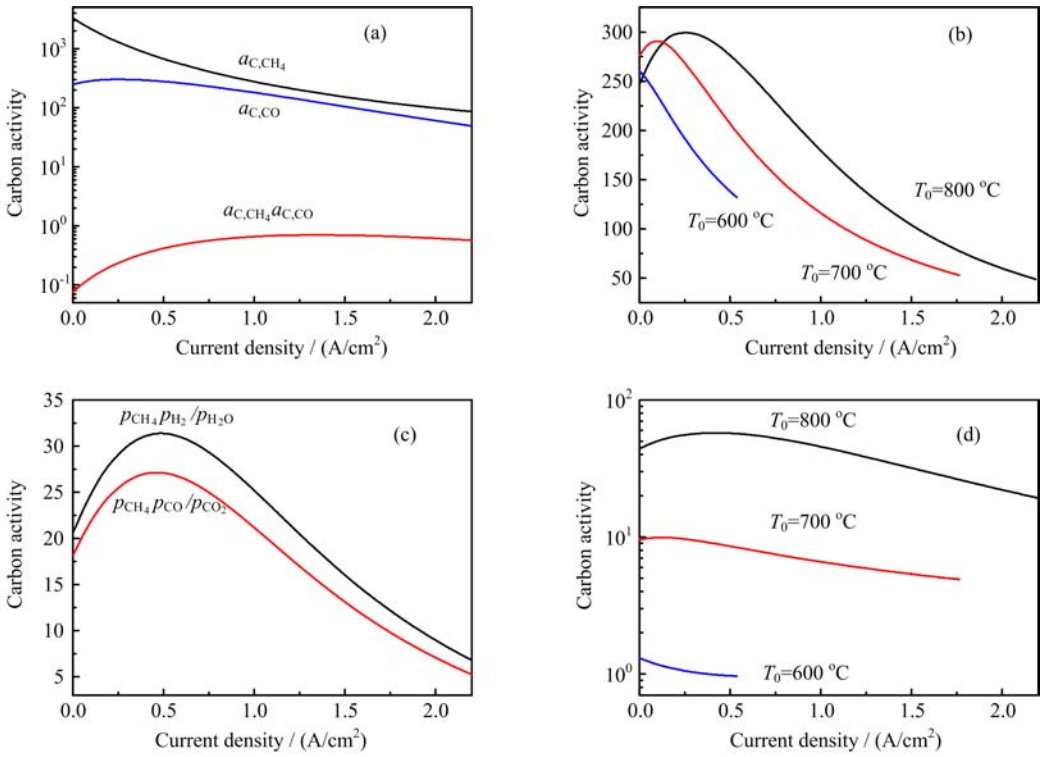

FIG. 8 Current density dependence of carbon activity at O_B. (a) Three different measures of carbon activity at T_0=800 °C. (b) Variation of carbon activity, $a_C=a_{C,CH_4}a_{C,CO}$, with temperature. (c) Variation of carbon activity, a_{C^*}, with $p_{CH_4}p_{H_2}/p_{H_2O}$ and $p_{CH_4}p_{CO}/p_{CO_2}$ at T_0=800 °C. (d) Variation of carbon activity, $a^*_{C^*}$, with temperature.

a_{C,CH_4} and $a_{C,CO}$ can be calculated with the fuel compositions and temperature inside the anode obtained with the multi-physics numerical simulation.

Figure 8(a) shows the variations of a_{C,CH_4} and $a_{C,CO}$ at O_B with the cell current density. Generally, a_{C,CH_4} is much larger than 1, *i.e.*, strongly favoring carbon formation, but decreases rapidly with the current density due to the increase of p_{H_2} and decrease of p_{CH_4} (Fig.7). On the other hand, $a_{C,CO}$ is less than 1, *i.e.*, the corresponding reaction is helpful for coke cleaning, but increase with the current density. In other words, the two reactions have completely opposite effects regarding the carbon formation. Unfortunately, there is a lack of theory to express the overall effect of the two competing reactions.

One reasonable suggestion is to use $a_C=a_{C,CH_4}a_{C,CO}$ as the overall carbon activity [4, 11]. a_C at O_B is also shown in Fig.8(a). Overall, a_C decreases with the increasing output current, agreeing qualitatively with the experimental observations. However, a_C is still much larger than 1 for i_{out}=1.5 A/cm^2 when the carbon formation is clearly inhibited [6]. Therefore, a_C is not a good quantitative indicator for the carbon formation. Figure 8(b) shows the dependence of a_C on both tem-

DOI:10.1063/1674-0068/28/cjcp1503033

perature and current density. Considering the observations that the carbon formation is suppressed at 1.5, 1.0, and 0.5 A/cm^2 for T_0=800, 700, and 600 °C, respectively, a_C should be reduced by a factor of 100−200 to approach being a quantitative measure of carbon activity.

An alternative suggestion for the overall carbon activity has been proposed by some investigators [32−34]. It is argued that the carbon formation possibility is determined by the carbon coverage on the activated catalyst (Ni) surface. Based on the analysis of the elementary steps of reforming reaction, it is assumed that the chemisorbed carbon (C*) and the activated catalyst atom (*) are the most abundant reactive intermediates [34]. Consequently, the concentration of C* may be taken as the overall thermodynamic carbon activity, a_{C^*}. Via a pseudo-steady-state analysis, a_{C^*} is expressed as [34]:

$$\begin{aligned} a_{C^*} &= \frac{k_C p_{CH_4} p_{H_2}}{p_{H_2O}} \\ &= \frac{k'_C p_{CH_4} p_{CO}}{p_{CO_2}} \end{aligned} \tag{7}$$

where k'_C=$k_C K_{eq,WGS}$, k_C and k'_C are temperature-dependent variables with unknown explicit expressions. The equilibrium constant for the WGS reaction can be calculated as $1.767\times10^{-2}\exp(4400K/T)$ [26, 27] and is of the order of 1 for T=600−800 °C. Based on Eq.(7), a_{C^*} is proportional to $p_{CH_4}p_{H_2}/p_{H_2O}$ or $p_{CH_4}p_{CO}/p_{CO_2}$ at a given temperature [32−34]. The values of $p_{CH_4}p_{H_2}/p_{H_2O}$ and $p_{CH_4}p_{CO}/p_{CO_2}$ at O_B are shown in Fig.8(c). After passing a maximum at low current density, $p_{CH_4}p_{H_2}/p_{H_2O}$ and $p_{CH_4}p_{CO}/p_{CO_2}$ decrease with the increased current density, agreeing with the trend of current inhibition of carbon formation. Considering the carbon formation inhibition at 1.5 A/cm^2, k_C^{-1} should be about 20 bar at T_0=800 °C for a_{C^*} to be a quantitative measure of carbon activity.

It is tricky to determine the temperature-dependence of k_C (k'_C). As the methane decomposition is the major source of C*, it is suggested that the activation energy of methane decomposition may be used in the expression of the temperature-dependence of k_C. That is, a_{C^*} may be expressed as:

$$a_{C^*} = k_{catalyst} \frac{p_{CH_4} p_{H_2}}{p_{H_2O}} \exp\left(-\frac{E_a}{RT}\right) \tag{8}$$

where E_a=96.1 kJ/mol is the activation energy of methane decomposition, $k_{catalyst}$ is a constant representing the catalyst morphology. For convenience, a dimensionless variable $a^*_{C^*}$ may be used as the carbon activity [34],

$$\begin{aligned} a^*_{C^*} &= \frac{a_{C^*}}{k_{catalyst}} \\ &= \frac{p_{CH_4} p_{H_2}}{p_{H_2O}} \exp\left(-\frac{E_a}{RT}\right) \end{aligned} \tag{9}$$

$a^*_{C^*}$ at O_B is shown in Fig.8(d) for three fuel temperatures. It is seen that $a^*_{C^*}$ decreases significantly with the reduced temperature, in good accordance with the observed temperature dependence of coke formation [35]. Unfortunately, considering the current dependence of coke formation, $a^*_{C^*}$ should be reduced by a factor of >30, <10, and ∼1 for 800, 700, and 600 °C, respectively, in order for $a^*_{C^*}$ to be quantitatively representative of the carbon activity. In other words, $a^*_{C^*}$ is far from being ideal to represent the carbon activity.

From the above discussion, it is clear that none of the proposed carbon activity model is quantitatively correct. However, considering the scaling factor required for explaining the experimental results, relatively speaking, Eq.(9) is the best theoretical model, followed by Eq.(7), for the carbon activity.

D. Carbon activity for cell with an anode diffusion barrier layer

Numerical simulation has also been performed on the button cell with a diffusion barrier layer in the anode, as manufactured in Ref.[14]. The barrier layer is made of partially stabilized zirconia and CeO_2 that are both resistant to coking and barely activated for methane reforming. The thickness of the diffusion barrier layer is 500 μm. Like the cases shown in Fig.2, good agreements between the theoretical and experimental I-V relations are similarly obtained, further confirming the validity of our model. In the following, we focus on discussing the effect of the diffusion barrier layer on carbon activity. For convenience, the coking resistant diffusion barrier layer is referred as the barrier layer, while the rest of the anode is often referred as the anode in the following.

Figure 9 shows the partial pressures of fuel species on the cell symmetry axis for cells with and without the barrier layer. As shown in Fig.9, the barrier layer reduces the molar fraction of methane and increases the fraction of steam inside the anode, both are beneficial for coke removal. Both carbon activities, a_C and $a^*_{C^*}$, at O_B for cells with or without the barrier layer are compared in Fig.10. The variation patterns of both a_C and $a^*_{C^*}$ are similar. For relatively large current densities, a_C and $a^*_{C^*}$ with the barrier layer are much reduced compared to that without the barrier layer. This is attributed to the blocking effect of the inward methane diffusion and outward steam transport. The value of a_C ($a^*_{C^*}$) with no barrier layer at i_{out}=1.5 A/cm^2 is equivalent to that with the barrier layer at i_{out} of about 1−1.1 A/cm^2. This is in very good agreement with the experimental finding that the threshold current density for coking removal at T_0=800 °C is reduced from about 1.5 A/cm^2 with no barrier layer to about 1 A/cm^2 with the barrier layer [14]. In other words, the theoretical simulation provides a quantitative explanation of the experimental results. Meanwhile, it also shows that the carbon activity defined by a_C ($a^*_{C^*}$) is helpful for ana-

DOI:10.1063/1674-0068/28/cjcp1503033

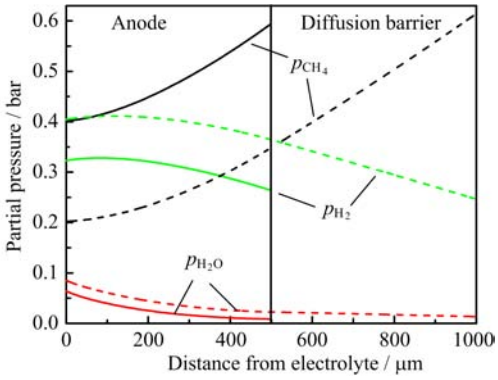

FIG. 9 Comparison of partial pressures of fuel species on the symmetry axis for cells with and without the anode diffusion barrier layer. Solid lines are without barrier, and dash lines are with barrier.

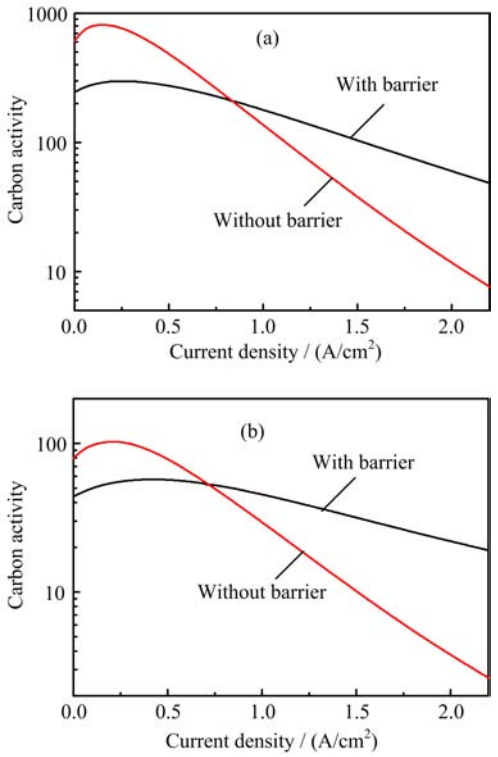

FIG. 10 Carbon activity at O_B as a function of the cell output current density: (a) a_C=$a_{C,CH_4}a_{C,CO}$, (b) $a^*_{C^*}$.

lyzing the propensity of carbon deposition even though, as discussed above, the value of a_C ($a^*_{C^*}$) does not correspond precisely to the true overall carbon activity. a_C ($a^*_{C^*}$) may be used for comparing the carbon activities of different operating conditions or different cell designs, or for finding out the most likely locations for carbon deposition.

IV. CONCLUSION

A multi-physics model is constructed for the analysis of methane fueled SOFCs. A novel feature of the model is to accurately describe the multi-component gas transport in porous anode with the DGMFM theory. The model is versatile and coupled with a generic rate expression for the methane steam reforming reaction.

The model is used to simulate the experimental SOFCs using low steam methane fuel. Excellent agreement between the theoretical and experimental *I-V* relations is obtained. The steam reaction order for the methane steam reforming with low steam content is accurately determined to be 1 by the high quality theoretical and experimental comparison. The result is remarkable considering the difficulty of low steam methane reforming experiment due to the deadly carbon deposition.

Detailed information about the distributions of physical quantities, *e.g.*, temperature, fuel species, reaction rate, heat flux, *etc.*, is obtained with the numerical simulation. Such information is very helpful for understanding the physical processes and improving cell design as well as optimizing operating conditions. In particular, the information is used for the analysis of carbon deposition that is vitally important for the SOFC technology. The modeling results provide a clear explanation for the role of operating current on inhibiting the carbon deposition.

Two main models for the effective overall carbon activity are analyzed in detail. The two models provide similar trends for the dependence of carbon activity on the current density. The corresponding temperature dependences are only similar qualitatively, but very different quantitatively. Compared to the experimental results on carbon deposition, both the models may be said to be qualitatively correct. However, both models are far from being ideal and more research is required to identify a quantitative measure of the carbon activity. The effect of diffusion barrier layer on the cell performance is discussed. The mechanism for the suppression of coke formation by the barrier layer is clearly illustrated. The reduction of the critical current density for avoiding coke formation by the diffusion layer is explained quantitatively by the two carbon activity models.

V. ACKNOWLEDGMENTS

This work was supported by the National Basic Research Program of China (No.2012CB215405), the National Natural Science Foundation of China (No.11374272), and the Specialized Research Fund for the Doctoral Program of Higher Education (No.20123402110064).

DOI:10.1063/1674-0068/28/cjcp1503033

[1] M. Andersson, J. Yuan, and B. Sundén, Appl. Energy **87**, 1461 (2010).
[2] M. Andersson, H. Paradis, J. Yuan, and B. Sundén, Int. J. Energy Res. **35**, 1340 (2011).
[3] M. Pillai, Y. Lin, H. Zhu, R. J. Kee, and S. A. Barnett, J. Power Sources **195**, 271 (2010).
[4] J. M. Klein, Y. Bultel, S. Georges, and M. Pons, Chem. Eng. Sci. **62**, 1636 (2007).
[5] M. Boder and R. Dittmeyer, J. Power Sources **155**, 13 (2006).
[6] J. Liu and S. A. Barnett, Solid State Ionics **158**, 11 (2003).
[7] J. Xu and G. F. Froment, AlChE J. **35**, 88 (1989).
[8] E. Ruckenstein and Y. H. Hu, Appl. Catal. A **133**, 149 (1995).
[9] K. Hou and R. Hughes, Chem. Eng. J. **82**, 311 (2001).
[10] E. S. Hecht, G. K. Gupta, H. Zhu, A. M. Dean, R. J. Kee, L. Maier, and O. Deutschmann, Appl. Catal. A **295**, 40 (2005).
[11] W. Sangtongkitcharoen, S. Assabumrungrat, V. Pavarajarn, N. Laosiripojana, and P. Praserthdam, J. Power Sources **142**, 75 (2005).
[12] M. D. Gross, J. M. Vohs, and R. J. Gorte, Electrochim. Acta **52**, 1951 (2007).
[13] S. P. Yoon, J. Han, S. W. Nam, T. H. Lim, and S. A. Hong, J. Power Sources **136**, 30 (2004).
[14] Y. Lin, Z. Zhan, and S. A. Barnett, J. Power Sources **158**, 1313 (2006).
[15] V. M. Janardhanan and O. Deutschmann, J. Power Sources **162**, 1192 (2006).
[16] S. Hosseini, K. Ahmed, and M. O. Tadé, J. Power Sources **234**, 180 (2013).
[17] W. Kong, J. Li, S. Liu, and Z. Lin, J. Power Sources **204**, 106 (2012).
[18] F. P. Nagel, T. J. Schildhauer, S. Biollaz, and S. Stucki, J. Power Sources **184**, 129 (2008).
[19] E. A. Mason and A. Malinauskas, *Gas Transport in Porous Media: the Dusty-Gas Model*, Amsterdam: Elsevier, (1983)
[20] R. Krishna and J. Wesselingh, Chem. Eng. Sci. **52**, 861 (1997).
[21] W. Kong, H. Zhu, Z. Fei, and Z. Lin, J. Power Sources **206**, 171 (2012).
[22] J. Li, W. Kong, and Z. Lin, J. Power Sources **232**, 106 (2013).
[23] D. Chen, W. Bi, W. Kong, and Z. Lin, J. Power Sources **195**, 6598 (2010).
[24] M. A. Khaleel, Z. Lin, P. Singh, W. Surdoval, and D. Collin, J. Power Sources **130**, 136 (2004).
[25] M. Zeppieri, P. Villa, N. Verdone, M. Scarsella, and P. De Filippis, Appl. Catal. A **387**, 147 (2010).
[26] Y. Wang, F. Yoshiba, M. Kawase, and T. Watanabe, Int. J. Hydrogen Energy **34**, 3885 (2009).
[27] Y. Yang, X. Du, L. Yang, Y. Huang, and H. Xian, Appl. Therm. Eng. **29**, 1106 (2009).
[28] J. Liu and S. A. Barnett, J. Am. Ceram. Soc. **85**, 3096 (2002).
[29] Y. Lin, Z. Zhan, J. Liu, and S. A. Barnett, Solid State Ionics **176**, 1827 (2005).
[30] H. Zhu and R. J. Kee, J. Power Sources **169**, 315 (2007).
[31] *COMSOL-Multiphysics, COMSOL Multiphysics/User's Guide Version* 3.5, Stokholm: COMSOL AB, (2008)
[32] S. Safvi, E. Bianchini, and C. Lund, Carbon **29**, 1245 (1991).
[33] I. Alstrup, M. Tavares, C. Bernardo, O. Sørensen, and J. Rostrup-Nielsen, Mater. Corros. **49**, 367 (1998).
[34] J. Wei and E. Iglesia, J. Catal. **224**, 370 (2004).
[35] C. M. Finnerty, N. J. Coe, R. H. Cunningham, and R. M. Ormerod, Catal. Today **46**, 137 (1998).

DOI:10.1063/1674-0068/28/cjcp1503033